Report

Cell Reports

Calcium-Activated Potassium Channels at Nodes of Ranvier Secure Axonal Spike Propagation

Graphical Abstract

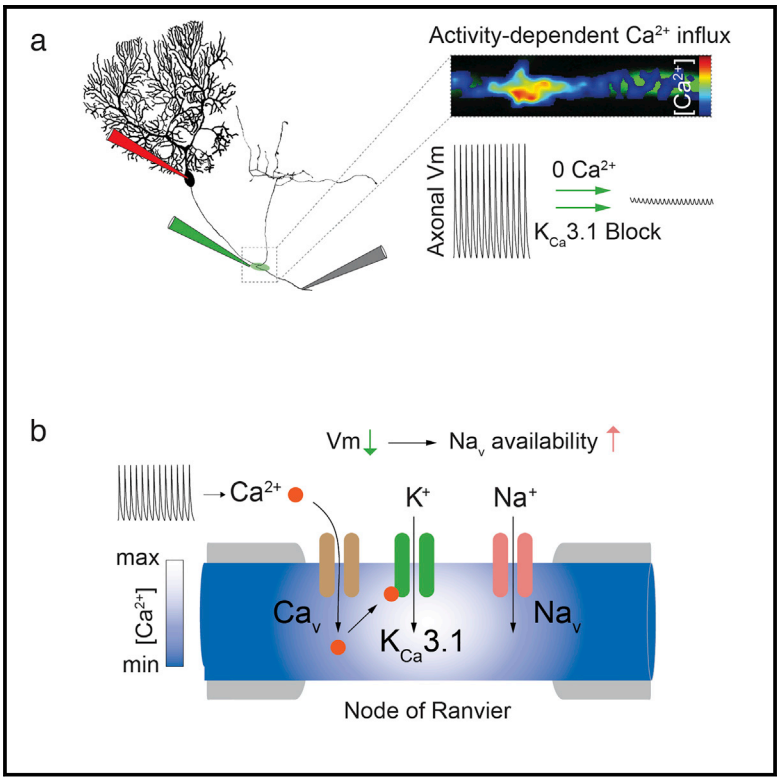

Highlights

- Activity-dependent node of Ranvier Ca^{2+} influx in Purkinje cell axons
- Ca_v and $K_{Ca}3.1$ channels required for axonal spike propagation
- Nodal $K_{Ca}3.1$ channels provide repolarizing drive to sustain axonal spike propagation

Authors

Jan Gründemann, Beverley A. Clark

Correspondence

b.clark@ucl.ac.uk

In Brief

Functional connectivity between brain regions relies on long-range signaling by myelinated axons. Gründemann and Clark show that local, activity-dependent calcium influx at nodes of Ranvier recruits calcium-activated potassium channels ($K_{Ca}3.1$) that drive repolarization and sustain node excitability, providing a pivotal mechanism to secure spike propagation along Purkinje cell axons.

Gründemann & Clark, 2015, Cell Reports *12*, 1715–1722
September 22, 2015
http://dx.doi.org/10.1016/j.celrep.2015.08.022

Cell Reports
Report

Calcium-Activated Potassium Channels at Nodes of Ranvier Secure Axonal Spike Propagation

Jan Gründemann[1,2] and Beverley A. Clark[1,*]
[1]Wolfson Institute for Biomedical Research, University College London, Gower Street, London WC1E 6BT, UK
[2]Present address: Friedrich Miescher Institute for Biomedical Research, Maulbeerstrasse 66, 4058 Basel, Switzerland
*Correspondence: b.clark@ucl.ac.uk
http://dx.doi.org/10.1016/j.celrep.2015.08.022

SUMMARY

Functional connectivity between brain regions relies on long-range signaling by myelinated axons. This is secured by saltatory action potential propagation that depends fundamentally on sodium channel availability at nodes of Ranvier. Although various potassium channel types have been anatomically localized to myelinated axons in the brain, direct evidence for their functional recruitment in maintaining node excitability is scarce. Cerebellar Purkinje cells provide continuous input to their targets in the cerebellar nuclei, reliably transmitting axonal spikes over a wide range of rates, requiring a constantly available pool of nodal sodium channels. We show that the recruitment of calcium-activated potassium channels (IK, $K_{Ca}3.1$) by local, activity-dependent calcium (Ca^{2+}) influx at nodes of Ranvier via a T-type voltage-gated Ca^{2+} current provides a powerful mechanism that likely opposes depolarizing block at the nodes and is thus pivotal to securing continuous axonal spike propagation in spontaneously firing Purkinje cells.

INTRODUCTION

Understanding information transmission within neuronal circuits, and the factors underlying long-range axonal signaling malfunction, relies on identifying the axonal ion channels that are key regulators of node of Ranvier (NoR) excitability. NoRs are highly specialized zones in myelinated axons containing high densities of voltage-gated sodium channels (Na_vs) and associated cytoskeletal complexes, creating active zones essential for saltatory conduction of action potentials (APs) (Debanne et al., 2011). The repolarizing currents required to sustain Na_v availability at NoRs for reliable AP transmission is less clear cut, particularly in the mammalian brain. Both low- and high-voltage-activated potassium (K^+) channel subunits (K_v7 and $K_v3.1/3$) have been anatomically localized to NoRs (Devaux et al., 2003, 2004; Pan et al., 2006), and although their presence can vary between brain regions and axon types (Debanne et al., 2011; Devaux et al., 2003, 2004), recent experiments provide direct evidence that K_v7 channels stabilize NoR membrane potential (Vm) in cortical L5 pyramidal cells (Battefeld et al., 2014) consistent with findings in peripheral nerve (Schwarz et al., 2006). The influence of delayed rectifier (DR) K^+ channels ($K_v1.1$ and $K_v1.2$), which are widely observed in the juxtaparanodal (JP) zone (Devaux et al., 2003; Ogawa et al., 2010; Rasband, 2010; Zhou et al., 1998), has, however, been difficult to assess without demyelination (Röper and Schwarz, 1989; Wilson and Chiu, 1990), and whether local Vm becomes sufficiently depolarized to recruit JP K_v1 channels during saltatory conduction is disputed (Arancibia-Carcamo and Attwell, 2014). Voltage-gated Ca^{2+} channels (Ca_vs), which could provide an additional source of depolarization as well as gating Ca^{2+}-dependent processes including recruitment of Ca^{2+}-dependent K^+ channels (K_{Ca}), have been described in central myelinated axons and shown to influence excitability at the axon initial segment (AIS) (Bender and Trussell, 2009; Bender et al., 2010; Yu et al., 2010). However, although Ca_vs have been proposed to influence NoR formation during development (Alix et al., 2008), their presence at mature NoRs in the brain is not established (Zhang et al., 2006).

Purkinje cells (PCs) in the cerebellum fire at high rates, both spontaneously and in response to synaptic input, and thus require fast recovery of sodium channels at their NORs. We have obtained direct evidence that, rather than solely relying on voltage-gated potassium channels, activity-dependent, spatially localized Ca^{2+} influx at NoRs of PC axons recruits an intermediate-type K_{Ca} (IK, or $K_{Ca}3.1$) to provide a node-specific repolarizing conductance crucial for axonal spike propagation.

RESULTS

Potassium Channels at Nodes of Ranvier

Using simultaneous somatic and axonal patch-clamp recordings, local pharmacology, and two-photon Ca^{2+} imaging of cerebellar PC axons, we directly investigated which ion channels are engaged at NoRs during AP propagation. We visualized PC axons in cerebellar slices by dye filling via the somatic recording pipette and recorded axonal APs downstream of NORs (see the Experimental Procedures; Figure 1A) identified by virtue of their presence at axonal branchpoints (Clark et al., 2005). APs are securely transmitted by PC axons at high firing rates, with failures occurring above ≈250 Hz (Khaliq and Raman, 2005; Monsivais et al., 2005). This propagation reliability is retained across axonal branchpoints, with equal limiting frequency in both the main projection axon (257 ± 17 Hz; also Monsivais et al., 2005)

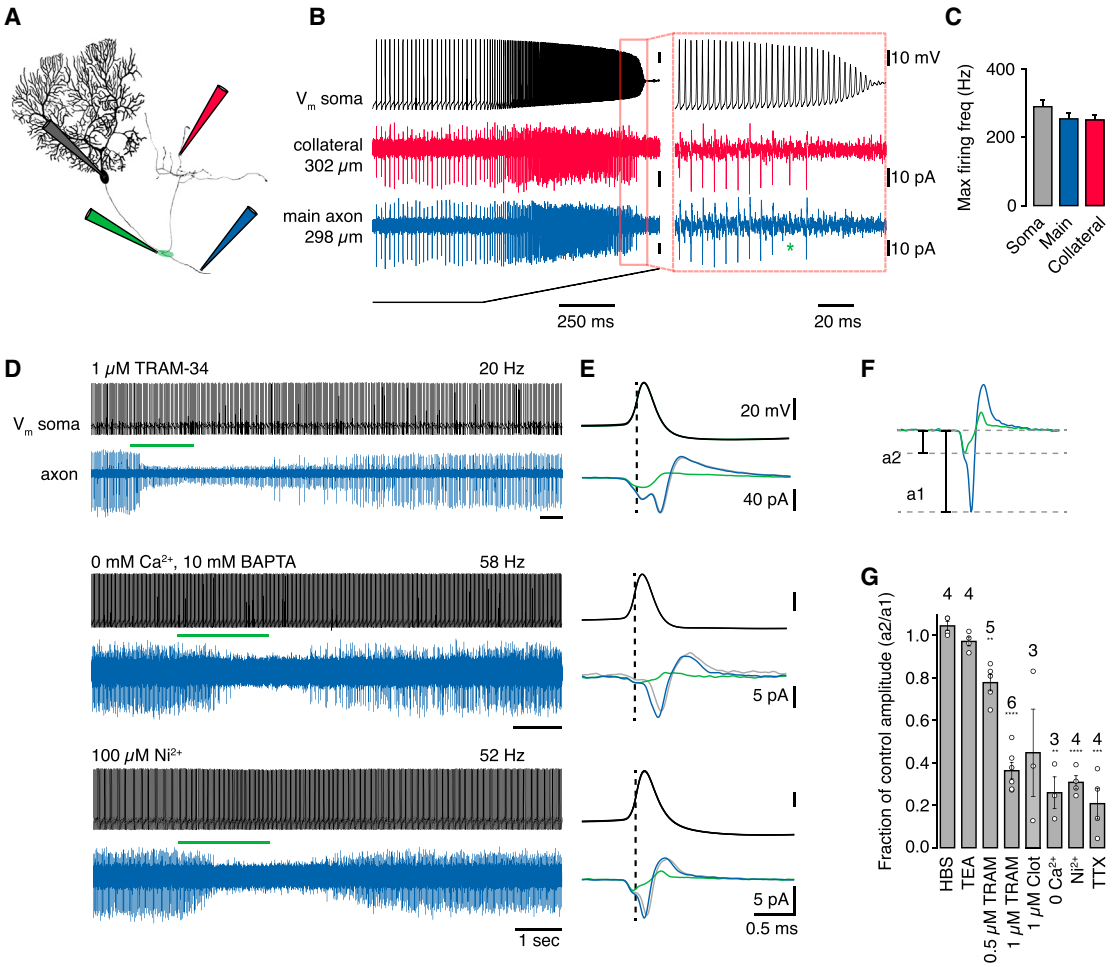

Figure 1. Highly Reliable Spike Propagation along Purkinje Cell Axons Is Secured by Node of Ranvier IK Channels

(A) Schematic of experimental configuration.

(B) Simultaneous whole-cell somatic and cell-attached axonal recordings of a spontaneously firing Purkinje cell in response to a somatic current ramp injection (2 nA). *Differentially propagated spike.

(C) Maximal firing frequencies at soma (292 ± 19 Hz, n = 19), main axon (257 ± 17 Hz, n = 9, includes data from Monsivais et al., 2005), and axon collateral (253 ± 14 Hz, n = 19).

(D) Local drug application (green bars) to branchpoint during whole-cell somatic recording (black) and cell-attached axonal recordings (blue) downstream of the targeted branchpoint. Baseline firing rate is indicated above somatic traces.

(E) Averaged whole-cell somatic and cell-attached spikes before (blue), during (green), and after (gray) drug application.

(F) Spike amplitude before (blue, a1) and during (green, a2) drug application.

(G) Data summary of axonal spike suppression.

$p < 0.0001$ for TRAM 1 μM, 0 Ca^{2+}, Ni^{2+}, $p < 0.005$ TRAM 500 nM, $p < 0.002$ TTX. TEA, HBS not significantly different from baseline (Student's t test). Error bars, ±SEM.

and in recurrent axon collaterals (Figures 1B and 1C, 253 ± 14 Hz, 0.05% differentially propagated spikes, n = 6 cells, see also Foust et al., 2010). We used local application (Figure S2A) of various ion channel antagonists to test their impact on AP propagation at NoRs in spontaneously firing PCs (firing rates 20–80 Hz). TTX (10 μM) completely blocked AP propagation, confirming the presence of a NoR at branchpoints (Figure S1D; see also Khaliq and Raman, 2005). In contrast, application of TEA at a concentration (10 mM) that should block a wide variety of K^+ channels including K_v1, K_v3, and K_v7 types (Grissmer et al., 1994; Hadley et al., 2000) did not affect AP propagation, having no impact on axonal capacitive current amplitude, firing rate, or conduction velocity (Figures S1B and S1C). This lack of effect was similar at high firing rates, and the limiting frequency for spike propagation was unchanged (Figure S1D). These results are unexpected given that TEA-sensitive K^+-channels are thought to contribute to axonal AP repolarization (Devaux et al., 2003; Hille, 1967; Röper and Schwarz, 1989), to stabilize nodal Vm as well as preventing antidromic spike reflection (Goldstein and Rall, 1974), and $K_v3.3$ subunits have been localized to PC axons (Chang et al., 2007). Potential explanations for these results might be that first, TEA-sensitive K^+ channels are absent

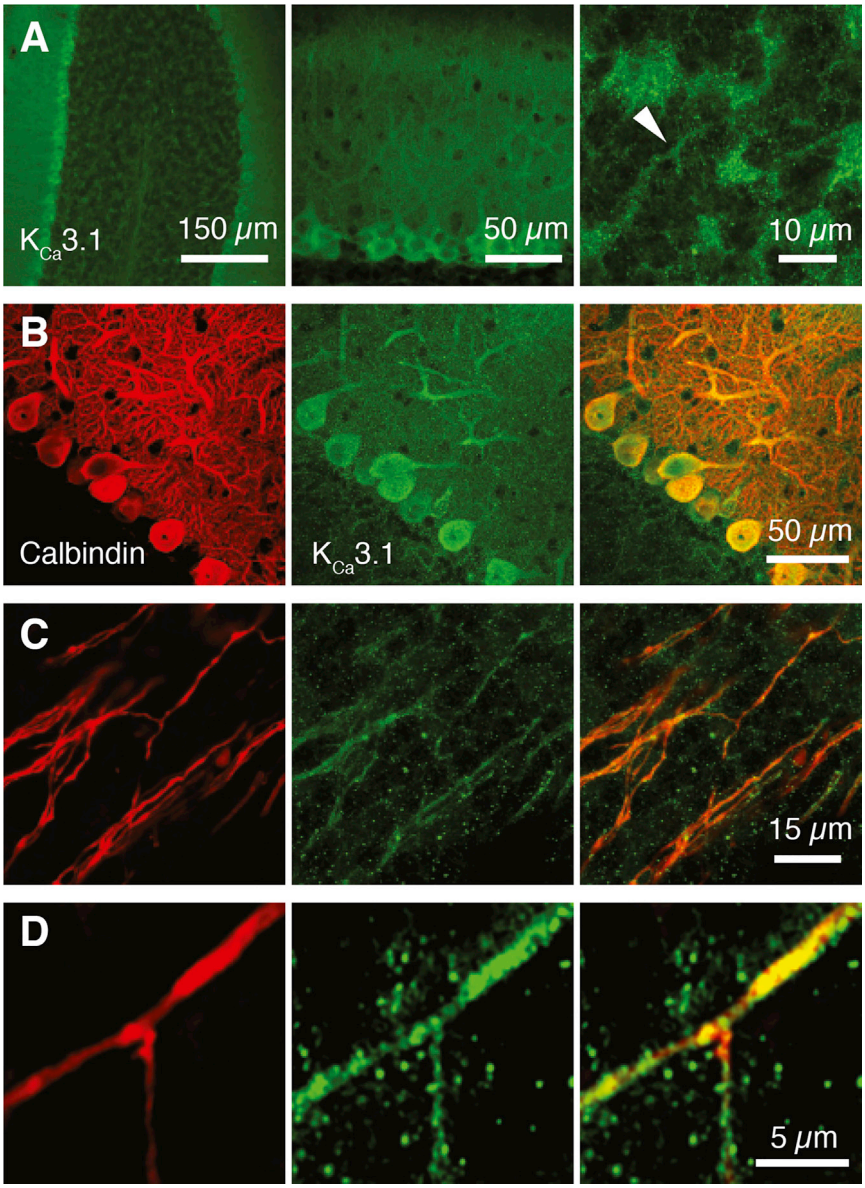

Figure 2. Expression of K_{Ca}3.1 in Purkinje Cell Axons

(A) Immunolabeling of K_{Ca}3.1 in cerebellar vermis (overview, left), PC soma, and dendrites (middle) and the center of the granule cell layer, which typically corresponds to the anatomical location where Purkinje cell axons have their first axonal branchpoint (70–100 μm) (right, arrowhead: potential axonal branchpoint).

(B) Co-immunolabeling of calbindin and K_{Ca}3.1 at PC somata and dendrites. Left, calbindin; Middle, K_{Ca}3.1; Right, merge. Maximum intensity projection.

(C) K_{Ca}3.1 staining along calbindin-positive axons in the granule cell layer. Maximum intensity projection.

(D) Calbindin-positive axonal branchpoint in the granule cell layer. Single optical plane, image deconvolved.

from PC axons and/or their NoRs and repolarization is mediated by an alternative mechanism. Second, they may be present but at insufficient density to be primary regulators of node excitability. Third, TEA-sensitive K^+ channels might be located behind tight myelin junctions in the juxtaparanodes (JPs) (Wang et al., 1993) and contribute to repolarization of the axonal membrane while being inaccessible to TEA, as observed in peripheral nerve (Chiu and Ritchie 1980; Kocsis and Waxman 1980) (however, see Mierzwa et al., 2010). Fourth, these channels may be present in the JPs but weakly activated by the limited Vm changes that are calculated to occur in healthy myelinated axon segments (Arancibia-Carcamo and Attwell, 2014).

Recently, an intermediate-type K_{Ca} conductance (IK, K_{Ca}3.1), not previously observed in the CNS and with a lower sensitivity to TEA (IC_{50} = 24 mM) (Wei et al., 2005), was described in cerebellar PCs and shown to contribute to postsynaptic integration (Engbers et al., 2012). We examined whether IK might provide an alternative mechanism for regulating excitability at NoRs and found that local application of the selective IK channel antagonist TRAM-34 (Engbers et al., 2012; Wulff et al., 2000) to axonal branchpoints led to a concentration-dependent block of axonal spike propagation during spontaneous firing (20–80 Hz; Figures 1D–1G), with no observed dependence on firing rate (R = 0.1). Clotrimazole (1 μM), another IK-selective blocker, had similar effects (Figure 1G), while apamin (1 μM) and iberiotoxin (1 μM), which block small (SK) and large (BK) K_{Ca} channels, respectively, had no impact (98% ± 0.44% [n = 5] and 97.3% ± 1.2% [n = 4] of control axonal spike amplitude). IK gating depends solely on intracellular $[Ca^{2+}]$ (K_d: 0.1–0.3 μM) (Wei et al., 2005; Joiner et al., 1997), and, since both local removal of extracellular Ca^{2+} and application of Ni^{2+} (100 μM) similarly suppressed action potential propagation (Figures 1D–1G), the activation of IK is likely initiated by Ca^{2+} influx via Ca_Vs. We confirmed that PC axons are immunopositive for the K_{Ca}3.1 subunit, the sole molecular entity that constitutes the IK channel, but found, surprisingly, that no hotspots were seen at NoRs and that K_{Ca}3.1 labeling was instead relatively uniform along the axon (Figure 2).

Activity-Dependent Ca^{2+} Influx at Nodes of Ranvier

Activity-dependent Ca^{2+} influx has been observed in optic nerve (Lev-Ram and Grinvald, 1987; Zhang et al., 2006), but the resulting Ca^{2+} transients are spatially uniform along both NoRs and internodes (Zhang et al., 2006), and the route of Ca^{2+} entry is uncertain. As yet, there is no direct evidence for Ca^{2+} influx localized to NoRs in the brain.

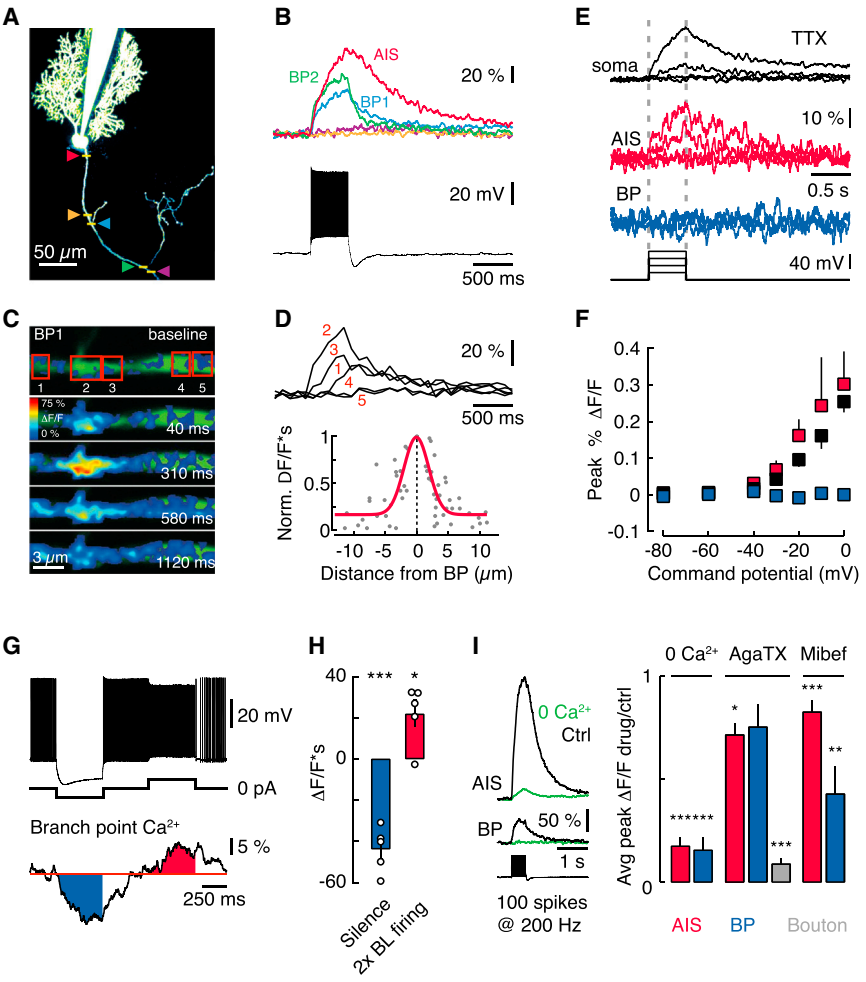

Figure 3. Local, Activity-Dependent Ca^{2+} Influx at Nodes of Ranvier

(A) Two-photon image of cerebellar Purkinje cell indicating line scan locations.

(B) Ca^{2+} transients (top, line scans) at locations shown in (A) during current-evoked spike trains (bottom). AIS, axon initial segment. BP1 and BP2, first and second axonal branchpoint.

(C) Frame-scan time series of BP1 during spike train. Green, axon morphology.

(D) Spike train-evoked ΔF/F at ROIs shown in (C) (red boxes). Normalized integrated ΔF/F (ΔF/F*s) against distance from an axonal branchpoint (bottom, n = 13 neurons).

(E) Soma, AIS, and first BP ΔF/F in response to 500-ms somatic voltage steps (voltage clamp) in bath-applied TTX (0.5 μM).

(F) Pooled data for max ΔF/F versus somatic command potential (soma, black; AIS, red; BP1, blue. n = 6 neurons).

(G) Activity-dependent changes in ΔF/F upon somatic current injection. Baseline holding current: 0 pA.

(H) Summary data for the change in ΔF/F*s during silence and activity (n = 5 cells).

(I) Ca^{2+} influx at the axon initial segment, first branchpoint and presynaptic boutons before and after bath application of 0 mM extracellular Ca^{2+} (n = 4), Agatoxin (AgaTX, n = 4, AIS = 3), and Mibefradil (Mibef, n = 9).

Error bars, ±SEM.

Using two-photon Ca^{2+}-imaging, we investigated whether the spatial distribution of calcium signals in PC axons might confer NoR specificity of IK recruitment. We detected prominent activity-dependent increases in intracellular Ca^{2+} concentration ($[Ca^{2+}]_i$) at NoRs (identified by their location at branchpoints) and at the AIS (see Bender and Trussell, 2009) during trains of evoked APs (Figures 3A–3C; 204 ± 21 Hz). Ca^{2+} signals were restricted to approximately 5 μm from the center of NoRs (Figures 3C and 3D), and there were no detectable changes in internodal $[Ca^{2+}]_i$ (Figure 3B), consistent with the lack of effect on spike propagation of 0 mM Ca^{2+}, 10 mM BAPTA application to the internodes (Figure S2B). $[Ca^{2+}]_i$ at NoRs required axonal APs, were suppressed when spontaneous firing was arrested by somatic hyperpolarization (Figure 3G), and could not be driven by somatic depolarization when spikes were blocked with bath-applied TTX (Figures 3E and 3F). Increases in $[Ca^{2+}]_i$ were spike rate dependent (Figure S3), slow, and cumulative and lead to sustained $[Ca^{2+}]_i$ during continuous activity (Figures 3G and 3H). $[Ca^{2+}]_i$ increase was also suppressed by removal of extracellular Ca^{2+} (16% ± 6% of control n = 4; Figure 3I) and bath application of mibefradil (Figures 3I and 5 μM, 43% ± 14% of control, p = 0.013) but was not sensitive to agatoxin IVa, which blocked Ca^{2+} transients in PC synaptic boutons as expected (Hillman et al., 1991) (Figures 3I; 9% ± 3% of control, $p < 0.0001$). This implies that T-type and not P-type Ca_Vs are the primary source of Ca^{2+} entry at NoRs. Additionally, although prior depolarization of the soma reduced $[Ca^{2+}]_i$ at the AIS, AP-triggered nodal Ca^{2+} signals were unaffected (Figures S3C and S3D), demonstrating that, in PCs, nodal $[Ca^{2+}]_i$ is independent of somatic Vm.

$K_{Ca}3.1$/IK Current Is Sufficient to Sustain Node Excitability

To understand the major impact of IK block on axonal AP propagation, we used a multicompartmental model of a PC (Clark et al., 2005) and tested whether IK, as the sole repolarizing conductance at the NoRs, can support reliable propagation of APs in a continuously firing axon (see the Experimental Procedures for details). At a minimum IK density of 0.05 S/cm^2, with an associated T-type Ca_V with a maximum permeability of 0.002 cm/s (Anwar et al., 2012) and an accompanying, low-density, juxtaparanodal DR K^+ conductance (0.002 S/cm^2, Clark et al., 2005) to mimic the Kv1.1/Kv1.2 channels commonly observed in immunohistochemical studies (Rasband 2010), AP propagation along the model axon was highly reliable. Complete removal of the IK conductance alone caused NoR depolarization, trapping of sodium channels in inactivated and blocked (Khaliq et al., 2003) states, and AP propagation block (Figure 4A).

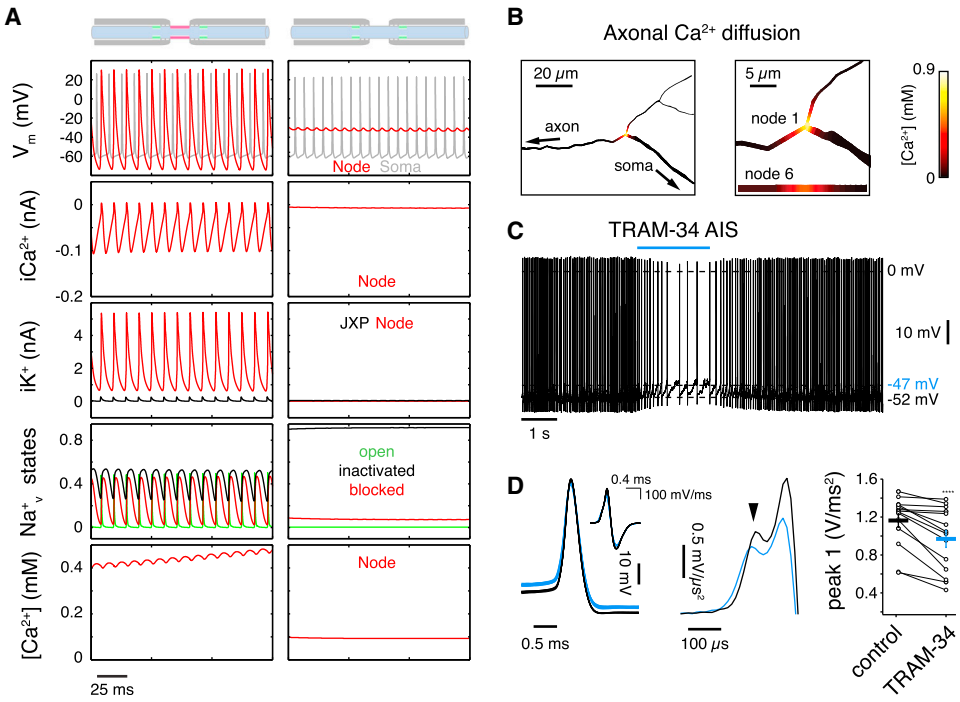

Figure 4. $K_{Ca}3.1$ Sets Node of Ranvier Membrane Potential and Preserves Nodal Excitability

(A) Data obtained from a PC multicompartmental model. NoR (red, sixth node, 1,820 μm from soma) and somatic (gray) APs (Vm, top row) during spontaneous firing in a Purkinje cell model with and without NoR $K_{Ca}3.1$ channels. Left column: AP propagation is sustained by nodal $gK_{Ca}3.1$ (0.05 S/cm^2) and juxtaparanodal (JP) delayed rectifier K^+ channels (0.002 S/cm^2). Right column: lack of axonal $K_{Ca}3.1$ causes depolarization block at the NoR. Second row: Ca^{2+} current at the NoR. Third row: total K^+ current at the JP and NoR, respectively, for each model. Fourth row: fractional resurgent Na_v states during spontaneous firing of each respective model. Bottom row: local Ca^{2+} concentration.

(B) Activity-dependent axonal Ca^{2+} diffusion in the model axon.

(C) Somatic recording from a spontaneously firing Purkinje cell during local application of 1 μM TRAM-34 to the AIS. TRAM-34 causes a depolarizing shift in Vm and a reduction of firing rate.

(D) Example APs (left) before (black) and during TRAM-34 (blue) application illustrate TRAM-34-induced change in Vm. Average second derivative of somatic APs (middle). Arrowhead indicates first peak originating in the axon. Summary data show a TRAM-induced reduction in the amplitude of the first axonal peak of the second derivative of the somatic action potential (right). Horizontal bars indicate average ±SEM (n = 15), $p < 0.0005$.

IK may therefore act to stabilize the NoR Vm during continuous firing and application of the IK channel inhibitor TRAM-34 (Figure 1) could cause depolarization block. Our observed lack of effect of TEA application to NoRs (Figure S1) implies that other K^+ channel types previously shown to be present in PC axons (Kv3.1, Chang et al., 2007) and NoRs ($K_v7.3$, Pan et al., 2006) may not, in the absence of IK, be sufficient to support AP propagation. A direct test of the hypothesis that IK stabilizes nodal Vm requires quantitative measurements of axonal Vm during IK block. Since PC NoRs are too small for patch-clamp recording and voltage-sensitive dye methods cannot be used to detect absolute changes in Vm, we used the AIS as a proxy for NoRs while recording spontaneous firing at the soma, presuming that some IK might be present there, as suggested by our immunohistochemistry data (Figure 2). During TRAM-34 application to the AIS, we observed a reduction in somatic firing rate of 25% ± 5.2% ($p < 0.001$, n = 15 cells, Figure 4C), accompanied by a small somatic depolarization (1.5 ± 0.2 mV, $p < 0.0001$) and an increase in AP threshold (1.8 ± 0.16 mV, $p < 0.0001$). In a minority of cells (4 / 15), TRAM-34 application to the AIS caused sufficient depolarization (ΔVm = 2.56 ± 1.28 mV, mean Vm = −48.4 ± 1.9 mV) to reversibly but completely block firing in some trials. Reduction of firing rate correlated with initial firing rate ($R = 0.53$, $p < 0.05$) so that cells with higher baseline rates showed a smaller reduction in spike rate on TRAM-34 application. This may reflect the presence of rate-dependent recruitment of BK and SK currents shown to regulate PC somatic Vm during spontaneous firing (Raman and Bean, 1999). Analysis of the second derivative of the somatic AP revealed a reduction in the component driven by current flow from the AIS (Figure 4D) as well as the local somatic component of the action potential during TRAM-34 application, indicating a reduced recruitment of sodium current at both locations.

DISCUSSION

K_{Ca} channels have been implicated in control of excitability in both unmyelinated (Lüscher et al., 1996) and myelinated (Lev-Ram and Grinvald, 1987) mammalian axons, although the evidence for the latter is indirect and the physiological impact unknown. Our results provide the first direct evidence for local, activity-dependent Ca_v-mediated Ca^{2+} influx at NoRs and for

the recruitment of an intermediate K_{Ca} current (IK, $K_{Ca}3.1$) that is an essential component for spike propagation. Our model indicates that IK alone can sustain the Na_v availability required for propagation security, although it is conceivable that other conductances might also play a role, for example, in setting the nodal Vm in the absence of firing. The sensitivity of AP conduction to low concentrations of Ni^{2+} and the suppression of the Ca^{2+} transients by mibefradil is consistent with the involvement of a T-type Ca_v, as seen in association with dendritic IK in PCs (Engbers et al., 2012). During sustained firing, this channel type is expected to be largely inactivated but could provide a small window current for Ca^{2+} entry. This might be of advantage since, due to the higher affinity of IK for Ca^{2+} (Wei et al., 2005), a small Ca^{2+} influx can be effective but less expensive for an energetically demanding cellular compartment. IK may provide advantages over other K^+ channel types in axons that continuously transmit APs, often at high rates. IK lacks intrinsic voltage dependence and does not inactivate, but, by virtue of the activity dependence of Ca^{2+} influx, it could be recruited and sustained at levels controlled by mean spike rate. Its localized recruitment by Ca^{2+} may also be amplified by Ca^{2+}-induced Ca^{2+} release (Llano et al., 1994). It has recently been shown that PCs also express BK channels under the myelin in the paranode region (Hirono et al., 2015). These channels appear to become functionally relevant at firing frequencies above 100 Hz, suggesting that they may act as a complementary partner to IK under conditions when $[Ca^{2+}]_i$ is sufficient for their activation. In the absence of fast voltage-gated K^+ currents, APs at NoRs may also be broader, as generated by the model, than the exceptionally narrow somatic APs in PCs, potentially further facilitating Ca^{2+} entry at these sites. Besides its role in axonal electrogenesis, nodal Ca^{2+} influx could also be important in regulating NoR structure and functional properties. For example, activity-dependent local Ca^{2+} levels might be crucial to target and maintain Ca_vs (Forti et al., 2000) and Na_vs (Hund et al., 2010) at NoRs (Wang et al., 2007) and to preserve or modify nodal architecture and myelin distribution (Alix et al., 2008; Einheber et al., 1997). Ca^{2+} signaling is thought to underlie the activity-dependent changes in mitochondrial motility observed in mammalian axons (Chiu, 2011), notably in PCs (Ohno et al., 2011). Importantly, given their spike frequency dependence, NoR Ca^{2+} signals could provide a readout of neuronal circuit activity, which could result in Ca^{2+}-dependent axonal plasticity beyond the AIS (Grubb and Burrone, 2010; Gründemann and Häusser, 2010; Kole, 2011; Kuba et al., 2010). In providing direct evidence for activity-dependent Ca^{2+} entry at NoRs and its recruitment of IK, our findings show that Ca^{2+} may play both short- and long-term roles in regulating axonal excitability, crucial for long-range signaling in neuronal circuits.

EXPERIMENTAL PROCEDURES

Electrophysiological Recordings

Methods used for preparing and recording from PCs and PC axons in cerebellar slices (200–250 μm) from P18–P43 C57Bl/6 mice were as previously described (Monsivais et al., 2005) and carried out under institutional and national approval. PC axons visualized by dye-filling and AP-associated cell-attached axonal capacitive currents were recorded in voltage clamp mode at 34°C ± 1°C. Amplitude of capacitive currents reflects the rate of rise of the axonal action potential and therefore pharmacological reduction in the amplitude reflects reduced sodium channel availability.

Drug Application

Drugs were diluted in ACSF and bath applied or diluted in HEPES-buffered or standard ACSF and pressure-applied locally via patch electrodes using a Picospritzer (0.5–10 psi, Parker). 30 μM Alexa Fluor 488 or 594 was included in the solution to help adjust pressure and pulse duration to target localized drug ejection. Ca^{2+} was replaced by Mg^{2+} in 0 mM Ca^{2+} solutions.

Two-Photon Ca^{2+} Imaging

Two-photon Ca^{2+} imaging and simultaneous electrophysiological recordings were performed using a custom-built dual galvanometer-based laser-scanning microscope (Prairie Technologies). A Ti:sapphire pulsed laser (MaiTai, Spectra Physics) tuned to 810 nm was used for two-photon excitation. 200 μM Oregon green 488 BAPTA-1 (OGB-1, Invitrogen) replaced EGTA in the pipette solution, which also contained 50 μM Alexa Fluor 594 hydrazide (Sigma-Aldrich) to visualize morphology. PCs were dialyzed for at least 15 min after establishing whole-cell mode before imaging.

Data Acquisition and Analysis

Data were digitized (ITC-18, InstruTECH, Heka) at 50–100 kHz and acquired using AxoGraph X (http://www.axographx.com/). Analysis was performed using custom-written routines in MATLAB (MathWorks) or IGOR Pro 6 (Wavemetrics) in combination with Neuromatic (http://www.thinkrandom.com/).

Two-photon imaging data were acquired with custom-written MATLAB software either as line scans (2 ms/line, 500 Hz) or as XYT frame scans for a chosen region of interest (5–20 frames/s), digitized with a BNC-2090 board (National Instruments), and analyzed with custom-written scripts in MATLAB, ImageJ, and IGOR Pro 6. Line scan and XYT frame-scan data were filtered using a boxcar running average or 2D-averaging filter, respectively. Relative changes in Ca^{2+}-sensitive fluorescence (OGB-1, ΔF/F) were calculated as raw fluorescence F_{raw} minus baseline fluorescence F_0 normalized to the background (F_B) subtracted baseline fluorescence (Yasuda et al., 2004): $\Delta F / F = F_{raw} - F_0 / F_0 - F_B$. In some cases, data are displayed as raw OGB-1 fluorescence values or relative changes in OGB-1 fluorescence normalized to the Alexa Fluor 594 red fluorescence (ΔF/R, Figure S3). Line scans are presented as averages of three consecutive trials.

Data are shown as mean ± SEM. Significance is tested using Student's t test unless otherwise stated, and a p value <0.05 is regarded as significantly different (InStat, GraphPad Software).

Immunohistochemistry and Confocal Microscopy

Mice were perfused with ice-cold PBS for 1 min and then with 4% paraformaldehyde (PFA) in PBS (10 min). Brains were dissected and 80 μm slices of cerebellar vermis were cut using a vibratome (Leica). Slices were washed in PBS and blocked in 10% goat serum for 2 hr before 48 hr antibody incubation in 2% goat serum ($K_{Ca}3.1$, mouse monoclonal, Santa Cruz Biotechnology, Calbindin D-28k, rabbit, Swant) followed by second antibody incubation for 24 hr (633 goat anti-rabbit, 488 as well as 633 goat anti-mouse, Invitrogen). Confocal image stacks were acquired using a 63× objective (NA 1.4, z-step: 130 nm, LSM700, Zeiss). High-magnification images of branchpoints were deconvolved with Huygens Software (SVI).

Multicompartmental Modeling

AP propagation along PC axons was simulated in NEURON using a previously published multicompartmental PC model (Clark et al., 2005), which included a resurgent sodium conductance typical of PCs (Khaliq et al., 2003). Additionally, at NoRs the model included a low-threshold Ca^{2+} conductance (Ca_vT, 0.002 cm/s) (Anwar et al., 2012) as well as an intermediate type K_{Ca} (IK, $K_{Ca}3.1$). Nodal $K_{Ca}3.1$ was based on a previously published BK conductance (Solinas et al., 2007), and its kinetics were adjusted to a four-state model to match previously published experimental recordings of IK (Bailey et al., 2010; Hirschberg et al., 1998). The nodal $K_{Ca}3.1$ current reversal potential was set to −80 mV. The simulations were run for 500 ms, and values shown in Figure 4 were measured at the center of the compartment.

SUPPLEMENTAL INFORMATION

Supplemental Information includes three figures and can be found with this article online at http://dx.doi.org/10.1016/j.celrep.2015.08.022.

AUTHOR CONTRIBUTIONS

J.G. and B.A.C. planned and performed experiments and wrote the manuscript.

ACKNOWLEDGMENTS

We thank Tiago Branco for discussion, technical advice, and two-photon acquisition software; Christoph Schmidt-Hieber and Arnd Roth for critical discussion; and Michael Häusser for discussion, support, and comments on the manuscript. Work was supported by grants from the Wellcome Trust (WT094077), the European Research Council (AdG 250345), and the Gatsby Charitable Foundation (GAT2919). J.G. was supported by the Wellcome Trust 4 year PhD Programme and an EMBO and Marie Curie Actions postdoctoral fellowship and is currently an Ambizione fellow of the Swiss National Science Foundation.

Received: March 30, 2015
Revised: June 22, 2015
Accepted: August 5, 2015
Published: September 3, 2015

REFERENCES

Alix, J.J.P., Dolphin, A.C., and Fern, R. (2008). Vesicular apparatus, including functional calcium channels, are present in developing rodent optic nerve axons and are required for normal node of Ranvier formation. J. Physiol. *586*, 4069–4089.

Anwar, H., Hong, S., and De Schutter, E. (2012). Controlling Ca^{2+}-activated K^+ channels with models of Ca^{2+} buffering in Purkinje cells. Cerebellum *11*, 681–693.

Arancibia-Carcamo, I.L., and Attwell, D. (2014). The node of Ranvier in CNS pathology. Acta Neuropathol. *128*, 161–175.

Bailey, M.A., Grabe, M., and Devor, D.C. (2010). Characterization of the PCMBS-dependent modification of KCa3.1 channel gating. J. Gen. Physiol. *136*, 367–387.

Battefeld, A., Tran, B.T., Gavrilis, J., Cooper, E.C., and Kole, M.H.P. (2014). Heteromeric Kv7.2/7.3 channels differentially regulate action potential initiation and conduction in neocortical myelinated axons. J. Neurosci. *34*, 3719–3732.

Bender, K.J., and Trussell, L.O. (2009). Axon initial segment Ca^{2+} channels influence action potential generation and timing. Neuron *61*, 259–271.

Bender, K.J., Ford, C.P., and Trussell, L.O. (2010). Dopaminergic modulation of axon initial segment calcium channels regulates action potential initiation. Neuron *68*, 500–511.

Chang, S.Y., Zagha, E., Kwon, E.S., Ozaita, A., Bobik, M., Martone, M.E., Ellisman, M.H., Heintz, N., and Rudy, B. (2007). Distribution of Kv3.3 potassium channel subunits in distinct neuronal populations of mouse brain. J. Comp. Neurol. *502*, 953–972.

Chiu, S.Y. (2011). Matching mitochondria to metabolic needs at nodes of Ranvier. Neuroscientist *17*, 343–350.

Chiu, S.Y., and Ritchie, J.M. (1980). Potassium channels in nodal and internodal axonal membrane of mammalian myelinated fibres. Nature *284*, 170–171.

Clark, B.A., Monsivais, P., Branco, T., London, M., and Häusser, M. (2005). The site of action potential initiation in cerebellar Purkinje neurons. Nat. Neurosci. *8*, 137–139.

Debanne, D., Campanac, E., Bialowas, A., Carlier, E., and Alcaraz, G. (2011). Axon physiology. Physiol. Rev. *91*, 555–602.

Devaux, J., Alcaraz, G., Grinspan, J., Bennett, V., Joho, R., Crest, M., and Scherer, S.S. (2003). Kv3.1b is a novel component of CNS nodes. J. Neurosci. *23*, 4509–4518.

Devaux, J.J., Kleopa, K.A., Cooper, E.C., and Scherer, S.S. (2004). KCNQ2 is a nodal K^+ channel. J. Neurosci. *24*, 1236–1244.

Einheber, S., Zanazzi, G., Ching, W., Scherer, S., Milner, T.A., Peles, E., and Salzer, J.L. (1997). The axonal membrane protein Caspr, a homologue of neurexin IV, is a component of the septate-like paranodal junctions that assemble during myelination. J. Cell Biol. *139*, 1495–1506.

Engbers, J.D.T., Anderson, D., Asmara, H., Rehak, R., Mehaffey, W.H., Hameed, S., McKay, B.E., Kruskic, M., Zamponi, G.W., and Turner, R.W. (2012). Intermediate conductance calcium-activated potassium channels modulate summation of parallel fiber input in cerebellar Purkinje cells. Proc. Natl. Acad. Sci. USA *109*, 2601–2606.

Forti, L., Pouzat, C., and Llano, I. (2000). Action potential-evoked Ca^{2+} signals and calcium channels in axons of developing rat cerebellar interneurones. J. Physiol. *527*, 33–48.

Foust, A., Popovic, M., Zecevic, D., and McCormick, D.A. (2010). Action potentials initiate in the axon initial segment and propagate through axon collaterals reliably in cerebellar Purkinje neurons. J. Neurosci. *30*, 6891–6902.

Goldstein, S.S., and Rall, W. (1974). Changes of action potential shape and velocity for changing core conductor geometry. Biophys. J. *14*, 731–757.

Grissmer, S., Nguyen, A.N., Aiyar, J., Hanson, D.C., Mather, R.J., Gutman, G.A., Karmilowicz, M.J., Auperin, D.D., and Chandy, K.G. (1994). Pharmacological characterization of five cloned voltage-gated K^+ channels, types Kv1.1, 1.2, 1.3, 1.5, and 3.1, stably expressed in mammalian cell lines. Mol. Pharmacol. *45*, 1227–1234.

Grubb, M.S., and Burrone, J. (2010). Activity-dependent relocation of the axon initial segment fine-tunes neuronal excitability. Nature *465*, 1070–1074.

Gründemann, J., and Häusser, M. (2010). Neuroscience: A plastic axonal hotspot. Nature *465*, 1022–1023.

Hadley, J.K., Noda, M., Selyanko, A.A., Wood, I.C., Abogadie, F.C., and Brown, D.A. (2000). Differential tetraethylammonium sensitivity of KCNQ1-4 potassium channels. Br. J. Pharmacol. *129*, 413–415.

Hille, B. (1967). The selective inhibition of delayed potassium currents in nerve by tetraethylammonium ion. J. Gen. Physiol. *50*, 1287–1302.

Hillman, D., Chen, S., Aung, T.T., Cherksey, B., Sugimori, M., and Llinás, R.R. (1991). Localization of P-type calcium channels in the central nervous system. Proc. Natl. Acad. Sci. USA *88*, 7076–7080.

Hirono, M., Ogawa, Y., Misono, K., Zollinger, D.R., Trimmer, J.S., Rasband, M.N., and Misonou, H. (2015). BK channels localize to the paranodal junction and regulate action potentials in myelinated axons of cerebellar Purkinje cells. J. Neurosci. *35*, 7082–7094.

Hirschberg, B., Maylie, J., Adelman, J.P., and Marrion, N.V. (1998). Gating of recombinant small-conductance Ca-activated K^+ channels by calcium. J. Gen. Physiol. *111*, 565–581.

Hund, T.J., Koval, O.M., Li, J., Wright, P.J., Qian, L., Snyder, J.S., Gudmundsson, H., Kline, C.F., Davidson, N.P., Cardona, N., et al. (2010). A β(IV)-spectrin/CaMKII signaling complex is essential for membrane excitability in mice. J. Clin. Invest. *120*, 3508–3519.

Joiner, W.J., Wang, L.Y., Tang, M.D., and Kaczmarek, L.K. (1997). hSK4, a member of a novel subfamily of calcium-activated potassium channels. Proc. Natl. Acad. Sci. USA *94*, 11013–11018.

Khaliq, Z.M., and Raman, I.M. (2005). Axonal propagation of simple and complex spikes in cerebellar Purkinje neurons. J. Neurosci. *25*, 454–463.

Khaliq, Z.M., Gouwens, N.W., and Raman, I.M. (2003). The contribution of resurgent sodium current to high-frequency firing in Purkinje neurons: an experimental and modeling study. J. Neurosci. *23*, 4899–4912.

Kocsis, J.D., and Waxman, S.G. (1980). Absence of potassium conductance in central myelinated axons. Nature *287*, 348–349.

Kole, M.H. (2011). First node of Ranvier facilitates high-frequency burst encoding. Neuron *71*, 671–682.

Kuba, H., Oichi, Y., and Ohmori, H. (2010). Presynaptic activity regulates Na(+) channel distribution at the axon initial segment. Nature *465*, 1075–1078.

Lev-Ram, V., and Grinvald, A. (1987). Activity-dependent calcium transients in central nervous system myelinated axons revealed by the calcium indicator Fura-2. Biophys. J. *52*, 571–576.

Llano, I., DiPolo, R., and Marty, A. (1994). Calcium-induced calcium release in cerebellar Purkinje cells. Neuron *12*, 663–673.

Lüscher, C., Lipp, P., Lüscher, H.R., and Niggli, E. (1996). Control of action potential propagation by intracellular Ca2+ in cultured rat dorsal root ganglion cells. J. Physiol. *490*, 319–324.

Mierzwa, A., Shroff, S., and Rosenbluth, J. (2010). Permeability of the paranodal junction of myelinated nerve fibers. J. Neurosci. *30*, 15962–15968.

Monsivais, P., Clark, B.A., Roth, A., and Häusser, M. (2005). Determinants of action potential propagation in cerebellar Purkinje cell axons. J. Neurosci. *25*, 464–472.

Ogawa, Y., Oses-Prieto, J., Kim, M.Y., Horresh, I., Peles, E., Burlingame, A.L., Trimmer, J.S., Meijer, D., and Rasband, M.N. (2010). ADAM22, a Kv1 channel-interacting protein, recruits membrane-associated guanylate kinases to juxtaparanodes of myelinated axons. J. Neurosci. *30*, 1038–1048.

Ohno, N., Kidd, G.J., Mahad, D., Kiryu-Seo, S., Avishai, A., Komuro, H., and Trapp, B.D. (2011). Myelination and axonal electrical activity modulate the distribution and motility of mitochondria at CNS nodes of Ranvier. J. Neurosci. *31*, 7249–7258.

Pan, Z., Kao, T., Horvath, Z., Lemos, J., Sul, J.-Y., Cranstoun, S.D., Bennett, V., Scherer, S.S., and Cooper, E.C. (2006). A common ankyrin-G-based mechanism retains KCNQ and NaV channels at electrically active domains of the axon. J. Neurosci. *26*, 2599–2613.

Raman, I.M., and Bean, B.P. (1999). Ionic currents underlying spontaneous action potentials in isolated cerebellar Purkinje neurons. J. Neurosci. *19*, 1663–1674.

Rasband, M.N. (2010). Clustered K^+ channel complexes in axons. Neurosci. Lett. *486*, 101–106.

Röper, J., and Schwarz, J.R. (1989). Heterogeneous distribution of fast and slow potassium channels in myelinated rat nerve fibres. J. Physiol. *416*, 93–110.

Schwarz, J.R., Glassmeier, G., Cooper, E.C., Kao, T.-C., Nodera, H., Tabuena, D., Kaji, R., and Bostock, H. (2006). KCNQ channels mediate IKs, a slow K^+ current regulating excitability in the rat node of Ranvier. J. Physiol. *573*, 17–34.

Solinas, S., Forti, L., Cesana, E., Mapelli, J., De Schutter, E., and D'Angelo, E. (2007). Computational reconstruction of pacemaking and intrinsic electroresponsiveness in cerebellar Golgi cells. Front. Cell. Neurosci. *1*, 2.

Wang, H., Kunkel, D.D., Martin, T.M., Schwartzkroin, P.A., and Tempel, B.L. (1993). Heteromultimeric K+ channels in terminal and juxtaparanodal regions of neurons. Nature *365*, 75–79.

Wang, H.-G., George, M.S., Kim, J., Wang, C., and Pitt, G.S. (2007). Ca^{2+}/calmodulin regulates trafficking of Ca(V)1.2 Ca^{2+} channels in cultured hippocampal neurons. J. Neurosci. *27*, 9086–9093.

Wei, A.D., Gutman, G.A., Aldrich, R., Chandy, K.G., Grissmer, S., and Wulff, H. (2005). International Union of Pharmacology. LII. Nomenclature and molecular relationships of calcium-activated potassium channels. Pharmacol. Rev. *57*, 463–472.

Wilson, G.F., and Chiu, S.Y. (1990). Ion channels in axon and Schwann cell membranes at paranodes of mammalian myelinated fibers studied with patch clamp. J. Neurosci. *10*, 3263–3274.

Wulff, H., Miller, M.J., Hansel, W., Grissmer, S., Cahalan, M.D., and Chandy, K.G. (2000). Design of a potent and selective inhibitor of the intermediate-conductance Ca^{2+}-activated K^+ channel, IKCa1: a potential immunosuppressant. Proc. Natl. Acad. Sci. USA *97*, 8151–8156.

Yasuda, R., Nimchinsky, E.A., Scheuss, V., Pologruto, T.A., Oertner, T.G., Sabatini, B.L., and Svoboda, K. (2004). Imaging calcium concentration dynamics in small neuronal compartments. Sci. STKE *2004*, pl5.

Yu, Y., Maureira, C., Liu, X., and McCormick, D. (2010). P/Q and N channels control baseline and spike-triggered calcium levels in neocortical axons and synaptic boutons. J. Neurosci. *30*, 11858–11869.

Zhang, C.-L., Wilson, J.A., Williams, J., and Chiu, S.Y. (2006). Action potentials induce uniform calcium influx in mammalian myelinated optic nerves. J. Neurophysiol. *96*, 695–709.

Zhou, L., Zhang, C.L., Messing, A., and Chiu, S.Y. (1998). Temperature-sensitive neuromuscular transmission in Kv1.1 null mice: role of potassium channels under the myelin sheath in young nerves. J. Neurosci. *18*, 7200–7215.

Cell Reports

Supplemental Information

Calcium-Activated Potassium Channels at Nodes of Ranvier Secure Axonal Spike Propagation

Jan Gründemann and Beverley A. Clark

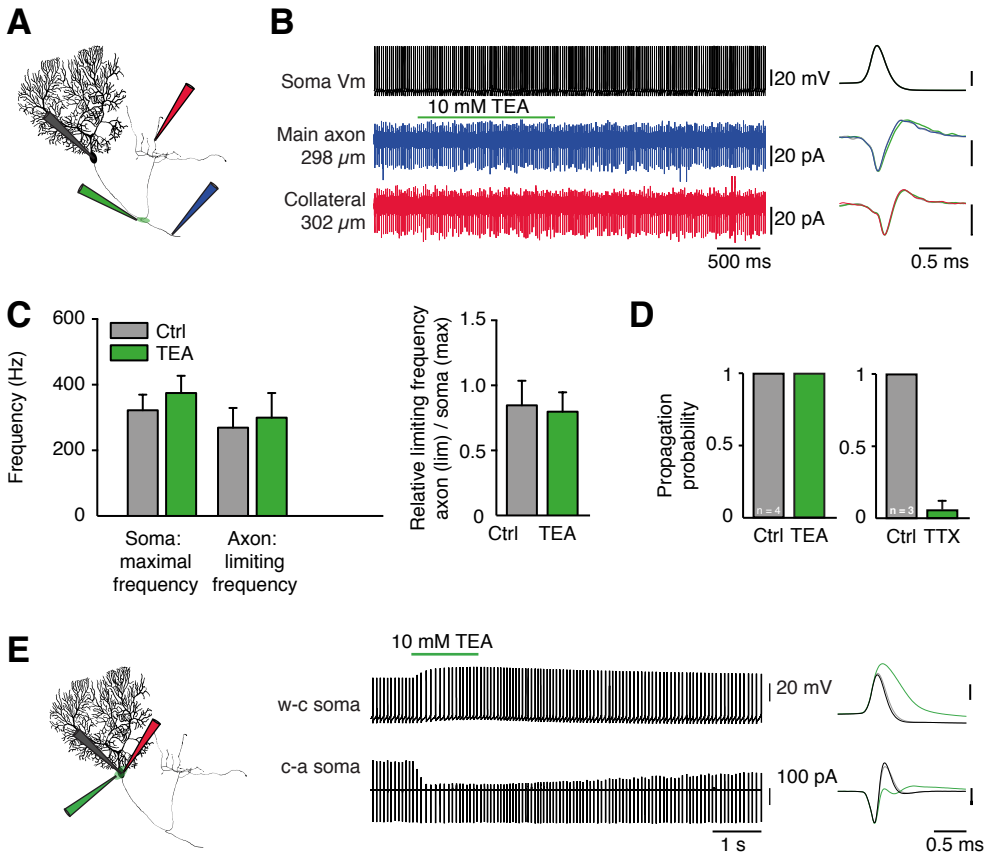

Supplementary Figure S1: TEA application to branch points lacks effect on axonal spike propagation along Purkinje cell axons. Related to Figure 1.

(**A, B**) Simultaneous whole-cell somatic and cell-attached axonal recording of a cerebellar Purkinje cell demonstrate lack of effect of local application of TEA (green) to axonal branch points. Right: Average axonal spike waveforms during control and TEA puff (green). (**C**) Summary data of the maximal spike frequency at the soma (ctrl: 322±24 Hz, TEA: 375±26 Hz, P = 0.1) and axon (ctrl: 269±30 Hz, TEA: 300±37 Hz, P = 0.2519) before (grey) and after (green) branch point TEA puff. No significant difference in maximal spike frequency at the soma or axon was observed during TEA puff. Ratio between limiting axonal and maximal somatic spike frequency (Ctrl: 0.85 ± 0.09; TEA: 0.80 ± 0.07, P = 0.35). (**D**) No change in spike propagation probability or axosomatic delay (TEA/ctrl = 1.0 ± 0.06) was observed upon TEA puff. However, local TTX application to the branch point blocked spike propagation (see also Khaliq et al., 2005). (**E**) Simultaneous recording of whole-cell and cell-attached somatic action potentials demonstrate strong drug effect of local TEA application on the somatic action potential waveform in both recording modes.

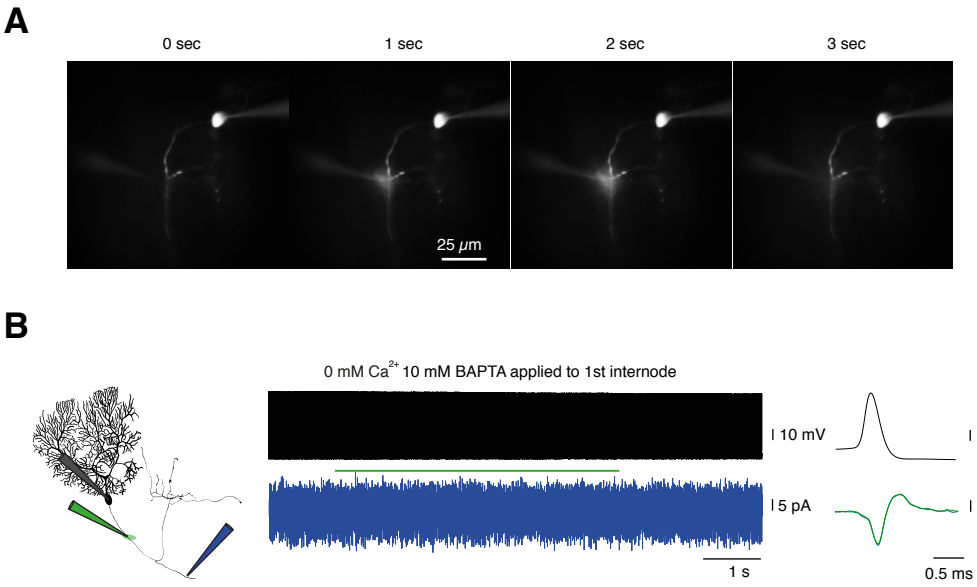

Supplementary Figure S2: Drug application is highly selective to targeted region and not effective at internodes. Related to Figure 1.

(**A**) Captured images during local 2 sec duration drug application to the axonal branch point of a labelled PC using a 5MΩ patch electrode and 2 psi ejection pressure. (**B**) Prolonged calcium removal from the internode region did not effect spike propagation n=3 $p<0.0001$ (example is same cell as in Fig 1D middle panel, in which BAPTA application to the branch point blocked spike propagation).

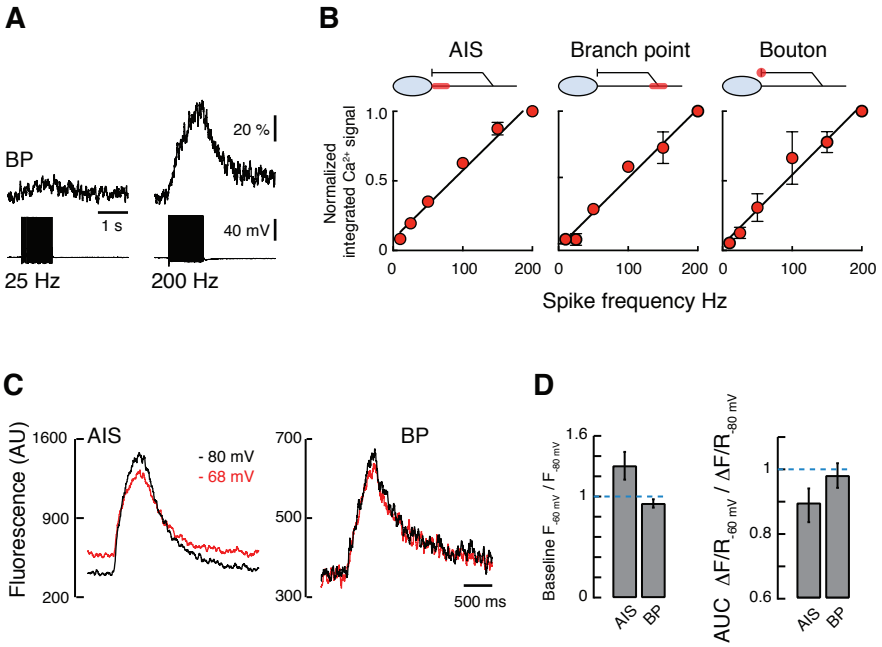

Supplementary Figure S3: Branch point Ca^{2+} levels are activity dependent, but not affected by somatic membrane potential history. Related to Figure 3.

(**A**) Ca^{2+} signals ($\Delta F/F$) at the first axonal BP (65 μm from soma) in response to a train of individually triggered spikes at 25 and 200 Hz. PCs were prevented from firing spontaneously by injection of hyperpolarizing current (V_m < -75 mV). (**B**) Correlation between the size of the Ca^{2+} signal (normalized to response at 200 Hz) and the frequency of individually triggered spikes at the axon initial segment (left, n = 7 cells), first branch point (middle, n = 6 cells) and presynaptic bouton of recurrent axon collaterals (right, n = 4 cells). (**C**) Raw Ca^{2+} indicator dye fluorescence signal (OGB1, arbitrary units, AU) at the axon initial segment (left, AIS) and first axonal branch point (right, BP, 82 μm) in response to 100 action potentials (200 Hz) triggered from two different somatic membrane potentials. Note the change in baseline fluorescence at the AIS in response to the somatic depolarization. (**D**) Summary data illustrating the dependence of the baseline Ca^{2+} fluorescence (left, AIS: ratio = 1.30 ± 0.14, P = 0.048, BP: ratio = 0.93, P = 0.115) and Ca^{2+} transient in response to 100 action potentials (right, AIS: ratio = 0.89 ± 0.05, P = 0.055, BP: ratio = 0.98, P = 0.623) on the somatic membrane potential at the AIS and BP (n = 12).